

A Comparison of *sun*, *ovate*, *fs8.1* and Auxin Application on Tomato Fruit Shape and Gene Expression

Yanping Wang^{1,2,3}, Josh P. Clevenger^{2,4,5}, Eudald Illa-Berenguer⁶, Tea Meulia⁷, Esther van der Knaap^{2,4,6,*} and Liang Sun^{1,2,8,*}

¹College of Horticulture, China Agricultural University, Beijing 100193, P.R. China

²Department of Horticulture and Crop Science, The Ohio State University/OARDC, Wooster, OH 44691, USA

³National Engineering Research Center for Vegetables, Beijing Academy of Agriculture and Forestry Sciences, Beijing 100097, P.R. China

⁴Institute of Plant Breeding, Genetics & Genomics, University of Georgia, Athens, GA 30602, USA

⁵Center for Applied Genetic Technologies, Mars Wrigley Confectionery, Athens, GA 30602, USA

⁶Center for Applied Genetic Technologies, University of Georgia, Athens, GA 30602, USA

⁷Department of Plant Pathology, Molecular and Cellular Imaging Center, The Ohio State University/OARDC, Wooster, OH 44691, USA

⁸Beijing Key Laboratory of Growth and Developmental Regulation for Protected Vegetable Crops, Department of Vegetable Science, College of Horticulture, China Agricultural University, Beijing 100193, P.R. China

*Corresponding authors: Liang Sun, E-mail, liang_sun@cau.edu.cn; Fax, 086-010-62731014; Esther van der Knaap, E-mail, EsthervanderKnaap@uga.edu; Fax, 001-706-583-0881.

(Received September 5, 2018; Accepted February 7, 2019)

Elongated tomato fruit shape is the result of the action of the fruit shape genes possibly in coordination with the phytohormone auxin. To investigate the possible link between auxin and the fruit shape genes, a series of auxin (2,4-D) treatments were performed on the wild-type and the fruit shape near-isogenic lines (NILs) in *Solanum pimpinellifolium* accession LA1589 background. Morphological and histological analyses indicated that auxin application approximately 3 weeks before anthesis led to elongated pear-shaped ovaries and fruits, which was mainly attributed to the increase of ovary/fruit proximal end caused by the increase of both cell number and cell size. Fruit shape changes caused by *SUN*, *OVATE* and *fs8.1* were primarily due to the alterations of cell number along different growth axes. Particularly, *SUN* caused elongation by extending cell number along the entire proximal-distal axis, whereas *OVATE* caused fruit elongation in the proximal area, which was most similar to the effect of auxin on ovary shape. Expression analysis of flower buds at different stages in fruit shape NILs indicated that *SUN* had a stronger impact on the transcriptome than *OVATE* and *fs8.1*. The *sun* NIL differentially expressed genes were enriched in several biological processes, such as lipid metabolism, ion transmembrane and actin cytoskeleton organization. Additionally, *SUN* also shifted the expression of the auxin-related genes, including those involved in auxin biosynthesis, homeostasis, signal transduction and polar transport, indicating that *SUN* may regulate ovary/fruit shape through modifying the expression of auxin-related genes very early during the formation of the ovary in the developing flower.

Keywords: Auxin • Fruit shape • *fs8.1* • *OVATE* • *SUN* • Tomato.

Abbreviations: CCD, charged-coupled device; DEGs, differentially expressed genes; DPI, days post flower initiation; NILs,

near-isogenic lines; dpi, dots per inch; OFP, OVATE family protein; PCA, principal component analysis; RPKM, reads per kilobase of exon model per million mapped reads; TCA, tricarboxylic acid; WBA, weeks before anthesis.

Introduction

Fruits of plants in the Angiosperm phylum are derived from gynoecia that originate from the fourth and final whorl in the floral meristem (Van der Knaap and Østergaard 2017). Some characteristics of the fruit are determined during floral development such as fruit structure and morphology, whereas others are determined later in development (Muños et al. 2011, Sun et al. 2015, Eldridge et al. 2016). Fruit shape is an important trait in horticultural plants, which does not only satisfy humans' curiosities, but also distinguishes varieties within a particular crop species. In tomato, large fasciated fruits are popular for slicing at home and in restaurants, while elongated and slightly blocky fruits are favored by the processing industry since they are easier to be harvested and processed mechanically than round-shaped fruits (Van der Knaap et al. 2014, Sun et al. 2017).

Fruit elongation in tomato is primarily controlled by four loci comprising *sun*, *ovate*, *sov1* and *fs8.1*. The genes underlying *sun*, *ovate* and *sov1* have been cloned (Liu et al. 2002, Xiao et al. 2008, Sun et al. 2015, Wu et al. 2018). *sun* is a gain-of-function mutation caused by a gene duplication mediated by a retrotransposition event, which leads to high expression of *SUN* (Xiao et al. 2008). *SUN* encodes a member of IQ67-domain (IQD) family, which are involved in Ca²⁺ signal transduction and cellular trafficking through interacting with calmodulins (CaMs) and kinesin-light chain-related protein (Xiao et al. 2008, Bürstenbinder et al. 2013, Clevenger et al. 2015). Recent studies in Arabidopsis show that most of the IQDs co-locate with microtubules (MTs) where they are proposed to regulate

MT organization and cell shape with MT-binding proteins (Bürstenbinder et al. 2017, Wendrich et al. 2018). Certain IQDs also respond to auxin treatment at the transcriptional level and may function as scaffolds linking auxin and calcium signaling with MT (Bürstenbinder et al. 2017, Wendrich et al. 2018). In tomato, *SUN* has also been linked to Ca^{2+} signaling (Clevenger et al. 2015). For *ovate*, the null mutation often leads to an oval-shaped fruit and encodes a member of the OVATE family protein (OFP) class (Liu et al. 2002). OVATE interacts with certain members of TONNEAU1 Recruiting Motif (TRM) superfamily and is proposed to regulate MT organization and ultimately cell division patterns (Van der Knaap et al. 2014, Lazzaro et al. 2018, Wu et al. 2018). Recently, another member of the tomato OFP family, *SIOFP20*, was cloned and found to underlie the *sov1* (*suppressor of ovate*) locus. *sov1* synergistically interacts with *ovate* leading to a pear-shaped tomato (Wu et al. 2018). *sov1* is likely the result of a 31-kb deletion in the upstream regulatory region of *OFP20*, which leads to lower expression of the gene and an elongated fruit (Wu et al. 2018). *fs8.1* has been fine-mapped to a ~3 Mb region on the long arm of chromosome 8 but the underlying gene(s) is still unknown (Sun et al. 2015). Morphological and histological analyses have implied that genes underlying these four tomato fruit elongation loci regulate primarily cell division along different growth axes during development (Wu et al. 2011, Sun et al. 2015, Van der Knaap and Østergaard 2017, Wu et al. 2018). However, how interaction with MT of *SUN*, *OVATE*, *SIOFP20* and potentially the protein(s) underlying *fs8.1* regulate fruit shape by cell division patterning is largely unknown.

Phytohormones, especially auxin and gibberellins, are associated with changes in fruit shape. In Arabidopsis, an intricate auxin transport model is proposed for gynoecium development and fruit formation (Nemhauser et al. 2000, Sohlberg et al. 2006, Ståldal et al. 2008, Larsson et al. 2014). Additionally, mutations and transgenic manipulation of specific auxin signaling components such as *ARF* and *Aux/IAA* genes, lead to the development of parthenocarpic and abnormally shaped fruit in both tomato and Arabidopsis (Wang et al. 2005, Goetz et al. 2007, De Jong et al. 2009, Damodharan et al. 2016, Ren et al. 2017). With regard to the tomato fruit shape genes, *SUN* overexpressor lines feature parthenocarpic fruits, increase of serration at the leaflet margins as well as twisted leaf rachises (Wu et al. 2011). This suggests alterations in auxin content, signaling and/or polar transport, even though no direct link has been found (Xiao et al. 2008, Wu et al. 2011, Clevenger et al. 2015). Interestingly, expression of certain Arabidopsis IQDs is up-regulated by auxin application (Wendrich et al. 2018), suggesting a link between certain IQD family members and this hormone. Moreover, the IAA level is significantly altered in young flower buds in the *fs8.1* background (Wu et al. 2015). Thus, the link between auxin and one or more of the known fruit shape genes seems plausible.

Solanum pimpinellifolium accession LA1589 features indeterminate growth, an abundant number of flowers and inflorescences as well as consistent floral development, and is therefore an ideal model for developmental studies (Xiao et al. 2009). The time from floral initiation to anthesis in LA1589 is 19 d, which is marked by 10 development landmarks

(Xiao et al. 2009). The stages include inflorescence formation and flower initiation [1 Days Post flower Initiation (DPI)], initiation of outermost perianth organs (2–3 DPI), initiation of inner perianth organs (4 DPI), stamen initiation (5 DPI), carpel initiation (6–7 DPI), microsporangia initiation (8 DPI), ovule initiation (9 DPI), male meiosis (10 DPI), female meiosis (11–13 DPI) and anthesis (19 DPI) (Xiao et al. 2009). In addition, near-isogenic lines (NILs) are powerful tools in both genetic and molecular studies (Chakrabarti et al. 2013, Clevenger et al. 2015, Mu et al. 2017, Biselli et al. 2018). We have introgressed the *sun*, *ovate* and *fs8.1* alleles into the LA1589 background to compare and contrast the effect of one or a combination of loci on morphological and physiological responses (Wu et al. 2015).

In this study, effects of exogenous auxin on altering tomato fruit shape were investigated in wild-type (WT), *sun* and *ovate* NILs at the morphological level. In addition, RNA-seq was performed on young flower buds of WT, *sun*, *ovate* and *fs8.1* NILs at different developmental stages. Our results demonstrate that exogenous auxin application at 2 to 3 weeks before anthesis (WBA) led to elongated anthesis-stage ovaries and altered fruit shape. This elongation effect was attributed to an increase of the ovary/fruit proximal end length, which was caused by the increase of both cell number and cell size, which appeared similar to the effect of a mutation in *OVATE*. The change of the ovary/fruit shape caused by *SUN*, *OVATE* and gene(s) underlying *fs8.1* were mainly attributed to the cell number changes along different growth axes. At the transcriptional level, *SUN* exhibited the strongest impact on shifting expression patterns whereas the other genes had less of an impact on the transcriptome. *SUN* may regulate the floral development as well as the ovary shape through altering genes involving in auxin signaling and polar transport, ion transmembrane transport, lipid metabolism and actin cytoskeleton organization.

Results

Exogenous auxin application at specific developmental stages led to elongated pear-shaped fruits in WT NIL

In addition to many roles, auxin is known to influence fruit shape (Wang et al. 2005, Goetz et al. 2007, De Jong et al. 2009, Damodharan et al. 2016, Ren et al. 2017). To determine the developmental aspects of auxin-induced fruit shape changes, 2,4-D was applied to WT NIL. We describe the resulting ovary and fruit shape based on how many weeks of 2,4-D application before anthesis (WBA). For example, if a flower opened at 3 weeks after treatment, fruits derived from this specific flower were called 3 WBA auxin-treated fruits. Compared to control, fruit shape index was significantly increased in 3 WBA auxin-treated fruits (Fig. 1A). When auxin was applied 2 WBA, the effect on shape was noticeable albeit not significant (Fig. 1A). In contrast, no change in shape was found when auxin was applied at other time points (Fig. 1A). More specifically, exogenous auxin clearly elongated the proximal end of the organ leading to pear-shaped fruits resembling the *ovate+sun* fruits (Fig. 1B, C) and fruits of the variety Yellow Pear

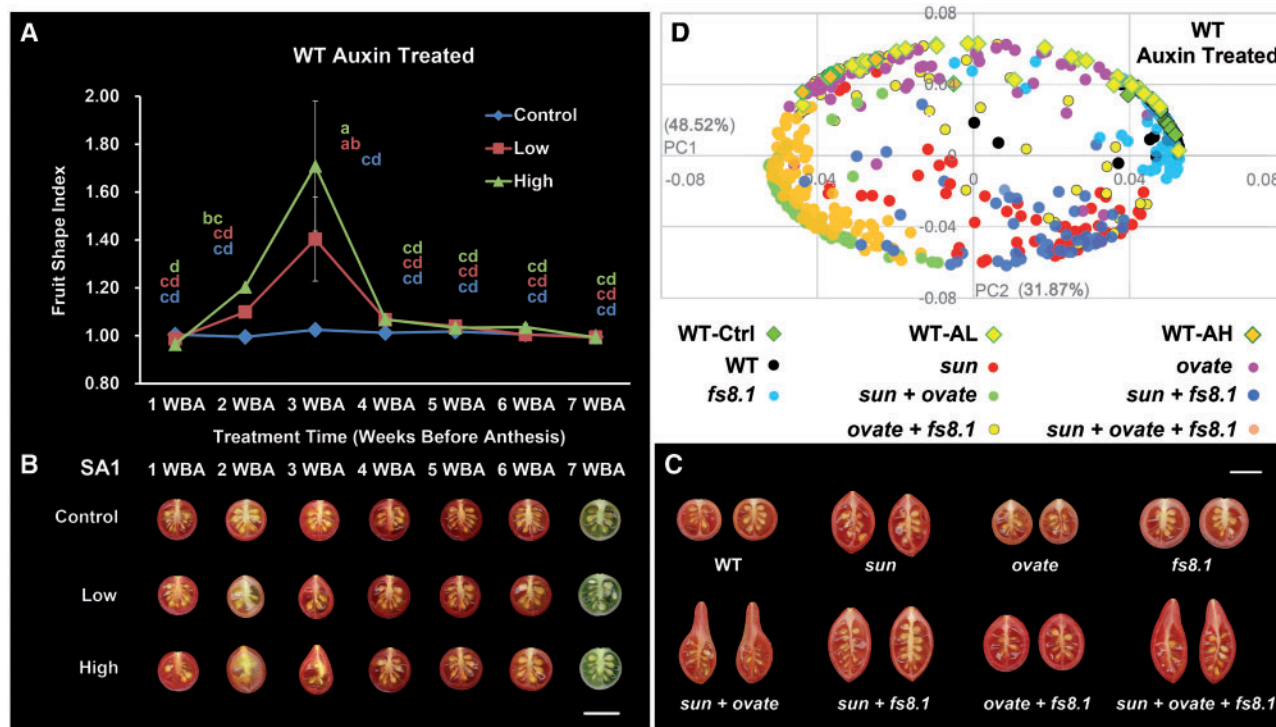


Fig. 1 Exogenous auxin elongated fruits of WT NIL in LA1589 background at certain developmental stages. (A) Fruit shape index changes after 2,4-D treatment. (B) Fruit shape changes after 2,4-D treatment. (C) Fruits of fruit shape NILs at ripening stage. (D) PCA of fruit shape attributes in fruit shape NILs and 3 WBA auxin-treated WT NIL. Statistical test in (A) was performed using Tukey HSD tests at 0.05 level. Scale bars in (B) and (C) represented 1 cm. Ctrl, AL and AH in (D) represented control, low concentration of auxin and high concentration of auxin, respectively.

which carries *ovate* and *sov1* (Rodríguez et al. 2013, Wu et al. 2018). To validate the classification of the auxin-treated fruits with *ovate*, PCA was performed between the 3 WBA auxin-treated and the three NILs using nine fruit shape attributes. PC1 and PC2, which together explained 80.4% of total variation, showed that the auxin-treated WT and *ovate* fruits clustered together (Fig. 1D), implying the similarity of the fruit shape in the auxin-treated WT and *ovate* NILs. In addition, exogenous auxin application of WT NIL of Sun1642 plants (*S. lycopersicum* background) led to seedless and rectangular fruits and not pear-shaped fruits (Supplementary Fig. S1), suggesting the effect of this hormone may also depend on the genetic background of plant materials.

Exogenous auxin application led to slender anthesis-stage ovaries in WT NIL

To clarify the morphological effect of exogenous auxin on fruit shape as well as to compare this effect with those of the fruit elongation loci, anthesis-stage ovaries were collected from WT, *sun*, *ovate*, *fs8.1*, 3 WBA auxin-treated WT NIL as well as *SUN* overexpressing lines, and sectioned except the *SUN* overexpressing lines (Fig. 2A–H; Supplementary Fig. S2A). *sun*, *SUN* overexpression lines, *ovate* and exogenous auxin treatments led to significantly increased ovary shape index when compared to untreated WT control (Table 1; Fig. 2A–D; Supplementary Fig. S2A). Specifically, *sun* led to increased anthesis-stage ovary shape index by increasing ovary maximum length,

which was mainly attributed to the elongation of the entire ovary wall (Table 1; Fig. 2B). Overexpression of *SUN* extremely slenderized the ovaries through primarily increasing the proximal end length and decreasing the width (Supplementary Fig. S2A). For *ovate*, the mutant allele increased the ovary shape index by simultaneously increasing maximal length and decreasing maximal width of the organ (Table 1; Fig. 2C). The increased ovary maximal length in the *ovate* NIL was attributed primarily to the elongation of the proximal end (Table 1). Compared to *sun* and *ovate*, exogenous auxin application led to even more slender ovaries which was similar to the effect of *SUN* overexpression, and the ovary shape index was almost twice that of *sun* or *ovate* (Table 1; Fig. 2F–H; Supplementary Fig. S2A). The increase in the final fruit shape index resulted from both the increase in ovary maximum length and the decrease in ovary maximum width (Table 1; Fig. 2F–H). In addition, detailed structural analysis revealed that the elongation of the proximal end of the organ was primarily contributing to the dramatically increased length of auxin-treated ovaries (Table 1). As to *fs8.1*, although shape index was not significantly affected, the ovary length and width were significantly increased leading to a larger organ (Table 1; Fig. 2D).

Exogenous auxin application affected cell number and size in anthesis-stage ovaries in WT NIL

To decipher a possible connection between auxin and one of the fruit shape genes, cell number and cell size were

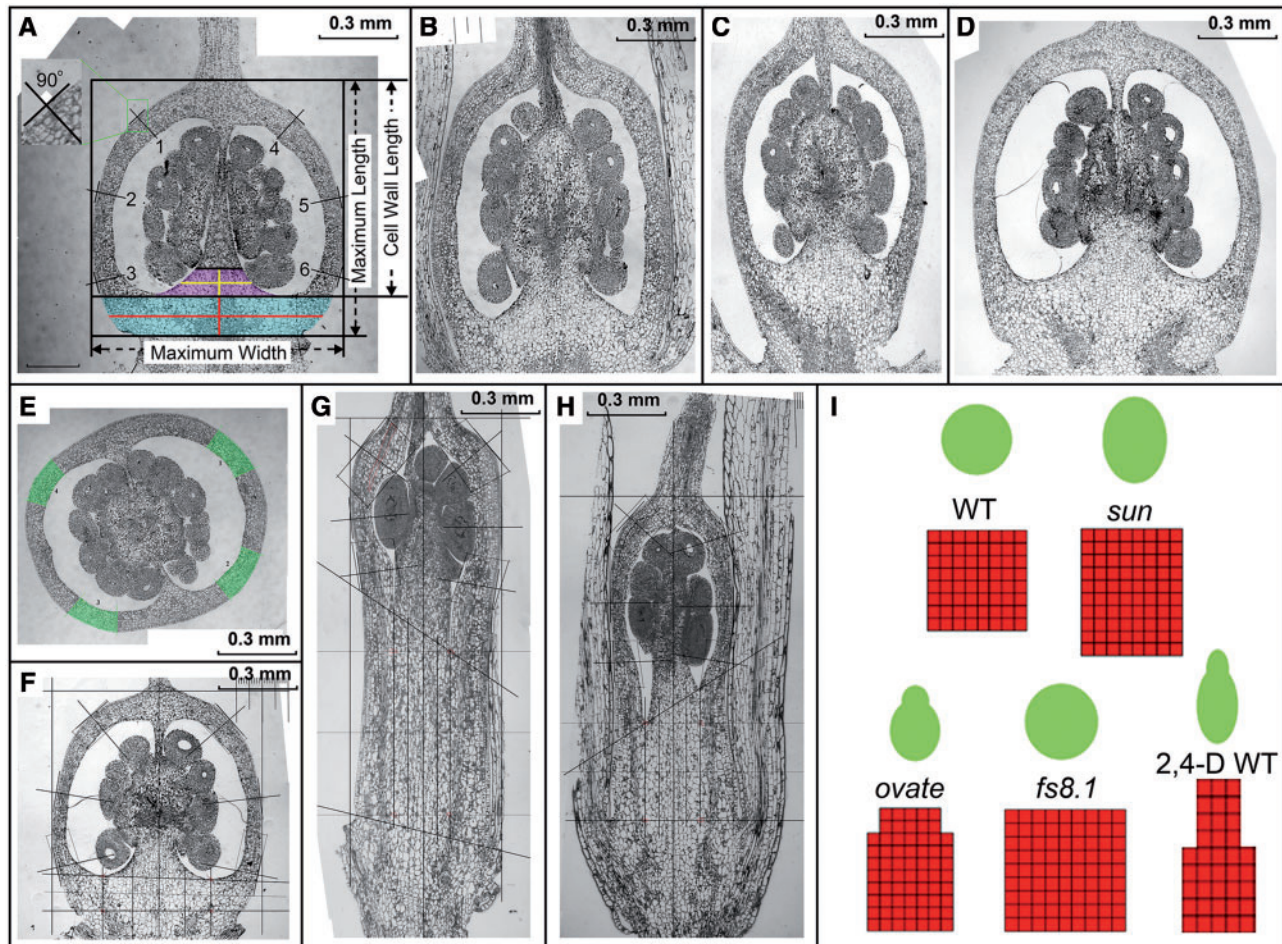


Fig. 2 Resin sections of WT, *sun*, *ovate*, *fs8.1* and 3 WBA auxin-treated WT ovaries at anthesis stage. (A–D) Resin sections of WT (A), *sun* (B), *ovate* (C) and *fs8.1* (D) ovaries at anthesis stage in proximal–distal direction. (E) Resin sections of WT ovaries at anthesis stage in medio-lateral direction. (F–H) Three WBA auxin-treated anthesis-stage ovaries (G, H) and control (F) in proximal–distal direction. (I) Models explaining the resulting ovary shapes by cell number, cell size and tissue type in the different NILs and after auxin treatment. Horizontal yellow, vertical yellow, horizontal red and vertical red lines in (A) indicated columella base width, columella base length, proximal end width and proximal end length, respectively. Purple and blue areas in (A) indicated the columella base and the proximal end, respectively.

Table 1 Morphological analyses of anthesis ovaries of *sun*, *ovate*, *fs8.1* and auxin-treated WT NIL

Parameter	Fruit shape NILs				2,4-D treated WT NIL		
	WT	<i>sun</i>	<i>ovate</i>	<i>fs8.1</i>	Control	Low	High
Proximal end length (mm)	0.15 ± 0.01 a	0.18 ± 0.01 a	0.27 ± 0.03 b	0.16 ± 0.01 a	0.11 ± 0.01 A	0.65 ± 0.14 B	0.37 ± 0.08 C
Proximal end width (mm)	0.76 ± 0.03 b	0.80 ± 0.01 ab	0.63 ± 0.01 c	0.86 ± 0.02 a	0.67 ± 0.01 A	0.50 ± 0.02 B	0.52 ± 0.02 B
Columella base length (mm)	0.14 ± 0.02 a	0.14 ± 0.01 a	0.16 ± 0.04 a	0.21 ± 0.01 a	n.a.	n.a.	n.a.
Columella base width (mm)	0.24 ± 0.02 a	0.34 ± 0.01 b	0.28 ± 0.02 a	0.28 ± 0.01 a	n.a.	n.a.	n.a.
Proximal end size (mm ²)	0.12 ± 0.01 a	0.14 ± 0.01 a	0.17 ± 0.03 a	0.15 ± 0.01 a	n.a.	n.a.	n.a.
Columella base size (mm ²)	0.04 ± 0.01 b	0.05 ± 0.01 ab	0.04 ± 0.01 b	0.07 ± 0.01 a	n.a.	n.a.	n.a.
Maximum length (mm)	1.00 ± 0.01 c	1.24 ± 0.03 ab	1.27 ± 0.02 a	1.18 ± 0.01 b	0.82 ± 0.03 A	1.43 ± 0.26 B	1.18 ± 0.08 B
Maximum width (mm)	0.97 ± 0.01 b	0.96 ± 0.02 b	0.89 ± 0.02 c	1.10 ± 0.01 a	0.80 ± 0.03 A	0.55 ± 0.05 B	0.57 ± 0.06 B
Ovary shape index	1.03 ± 0.01 c	1.30 ± 0.02 b	1.44 ± 0.04 a	1.07 ± 0.01 c	1.04 ± 0.08 A	2.59 ± 0.23 B	2.11 ± 0.37 B
Ovary wall length (mm)	0.85 ± 0.01 b	1.06 ± 0.03 a	1.00 ± 0.05 a	1.02 ± 0.01 a	0.71 ± 0.06 A	0.78 ± 0.14 AB	0.81 ± 0.01 B

Proximal end length and width and columella length and width were indicated by vertical red, horizontal red, vertical yellow and horizontal yellow lines in Fig.2A, respectively. Ovary shape index = Maximum length/Maximum width.

n.a., not analyzed. Statistical test was performed using Tukey HSD tests at 0.05 level.

investigated from microscopy sections of the ovary. As shown in **Table 2**, all three fruit elongation loci affected cell number of anthesis-stage ovaries albeit with different patterns. Particularly for *sun*, ovary wall cell number was significantly increased in proximal–distal direction and decreased in medio-lateral direction (**Table 2**) similar to previous findings (Wu et al. 2011). For *ovate*, the proximal end area was particularly affected. In this mutant, cell number at the proximal end was increased in proximal–distal direction, whereas cell number of ovary wall as well as the proximal end was decreased in medio-lateral direction (**Table 2**). Although ovary shape index was not noticeably changed in *fs8.1*, ovary wall cell number was significantly increased in proximal–distal direction and decreased in adaxial–abaxial direction of the entire organ (**Table 2**). Cell size was not significantly altered in the NILs although an increase was noted in the *ovate* NIL for all the tissues that were evaluated (**Table 2**). For auxin, exogenous application did not only impact cell number, but also changed cell size in nearly all tissues of the ovary, ultimately leading to an extreme elongated organ with a slender proximal end part (**Table 2; Fig. 2G, H**). Proximal end cell number was significantly increased in proximal–distal direction and decreased in the medio-lateral direction similar to *ovate* (**Table 2**). Even though cell number in the proximal–distal direction of the ovary wall was reduced, cell size was significantly increased by exogenous auxin application (**Table 2**). Based on the morphological and histological data, we developed models to explain the resulting ovary shapes by cell number, cell size and tissue type in the different NILs and after auxin treatment (**Fig. 2I**). Taken together, the data implied that auxin application and *ovate* resulted in similar ovary shapes.

Exogenous auxin application slenderized the proximal end in *sun* and *ovate* NIL fruits

To further explore the potential link between exogenous auxin and the fruit elongation loci on tomato fruit shape, we applied auxin to *sun* and *ovate* NILs inflorescences. Similar to what we observed in WT, exogenous auxin application at 2 and 3 WBA clearly increased fruit shape index in *sun* NIL, but showed no obvious effects at other time points (**Fig. 3A**). Auxin application to the *ovate* NIL showed a different response than WT or *sun* such that significant increases of fruit shape index were observed longer, namely when auxin was applied at 2, 3 and 4 WBA (**Fig. 3C**). With respect to fruit shape and structure, exogenous auxin did not only narrow the fruit proximal end, but also moved the locule to the distal end of the fruit in both *sun* and *ovate* NILs (**Fig. 3B, D**). In addition, distal fruit shapes showed that some auxin-treated fruits were elongated and pointy (**Fig. 3B, D**). Auxin application at 3 WBA in the *sun* and *ovate* NILs showed a shape similar to fruits of the *ovate+sun* double NIL and *SUN* overexpressing lines (**Fig. 1C**; Supplementary Fig. S2B). PCA analysis with the morphology of 3 WBA auxin-treated and triple NILs' fruits showed that exogenous auxin shifted the parameters of fruit shape of the *sun* NIL close to that of *sun+ovate* and *sun+ovate+fs8.1* NILs (**Fig. 3E**). Additionally, the 3 WBA auxin-treated *ovate* fruits

Table 2 Histological analyses of anthesis ovaries of *sun*, *ovate*, *fs8.1* and auxin-treated WT

Parameter	Fruit shape NILs				2,4-D treated WT NIL		
	WT	<i>sun</i>	<i>ovate</i>	<i>fs8.1</i>	Control	Low	High
	Proximal end cell size (μm^2)	279.02 ± 14.62 a	308.22 ± 4.53 a	339.10 ± 30.86 a	282.75 ± 20.87 a	242.97 ± 4.94 A	350.22 ± 23.99 B
Columella base cell size (μm^2)	179.53 ± 0.54 a	213.64 ± 3.63 a	210.06 ± 18.15 a	201.11 ± 5.15 a	n.a.	n.a.	n.a.
Proximal end cell number (P-D direction)	8.77 ± 0.23 a	9.47 ± 0.96 a	15.17 ± 1.75 b	9.05 ± 0.75 a	8.23 ± 0.90 A	27.93 ± 2.13 B	19.93 ± 0.80 C
Proximal end cell number (M-L direction)	50.5 ± 2.29 a	52.57 ± 1.66 a	41.90 ± 1.76 b	54.1 ± 1.60 a	51.33 ± 0.22 A	35.89 ± 1.67 B	38.38 ± 3.17 B
Ovary wall cell layer	12.01 ± 0.44 a	11.80 ± 0.16 a	10.93 ± 0.30 ab	10.48 ± 0.31 b	10.31 ± 0.03 A	10.33 ± 0.89 A	9.94 ± 0.33 A
Ovary wall cell number (P-D direction, 1/2 ovary)	85.68 ± 2.21 b	100.24 ± 1.09 a	88.96 ± 5.84 ab	100.50 ± 0.79 a	68.67 ± 0.72 A	46.39 ± 3.17 B	58.72 ± 2.56 C
Ovary wall cell size (P-D direction, μm^2)	112.17 ± 7.95 a	114.46 ± 11.92 a	116.97 ± 1.48 a	119.15 ± 3.74 a	119.58 ± 4.55 A	166.14 ± 15.33 B	137.4 ± 5.58 C
Ovary wall cell number (M-L direction, 1/2 ovary)	132.5 ± 3.52 a	119.25 ± 0.85 b	107.75 ± 6.02 b	133 ± 1.53 a	n.a.	n.a.	n.a.
Ovary wall cell size (M-L direction, μm^2)	138.95 ± 5.23 a	140.43 ± 7.49 a	159.46 ± 13.53 a	132.67 ± 6.16 a	n.a.	n.a.	n.a.

'P-D' and 'M-L' direction indicated 'proximal-distal' and 'medio-lateral' direction, respectively. n.a., not analyzed. Statistical test was performed using Tukey HSD tests at 0.05 level.

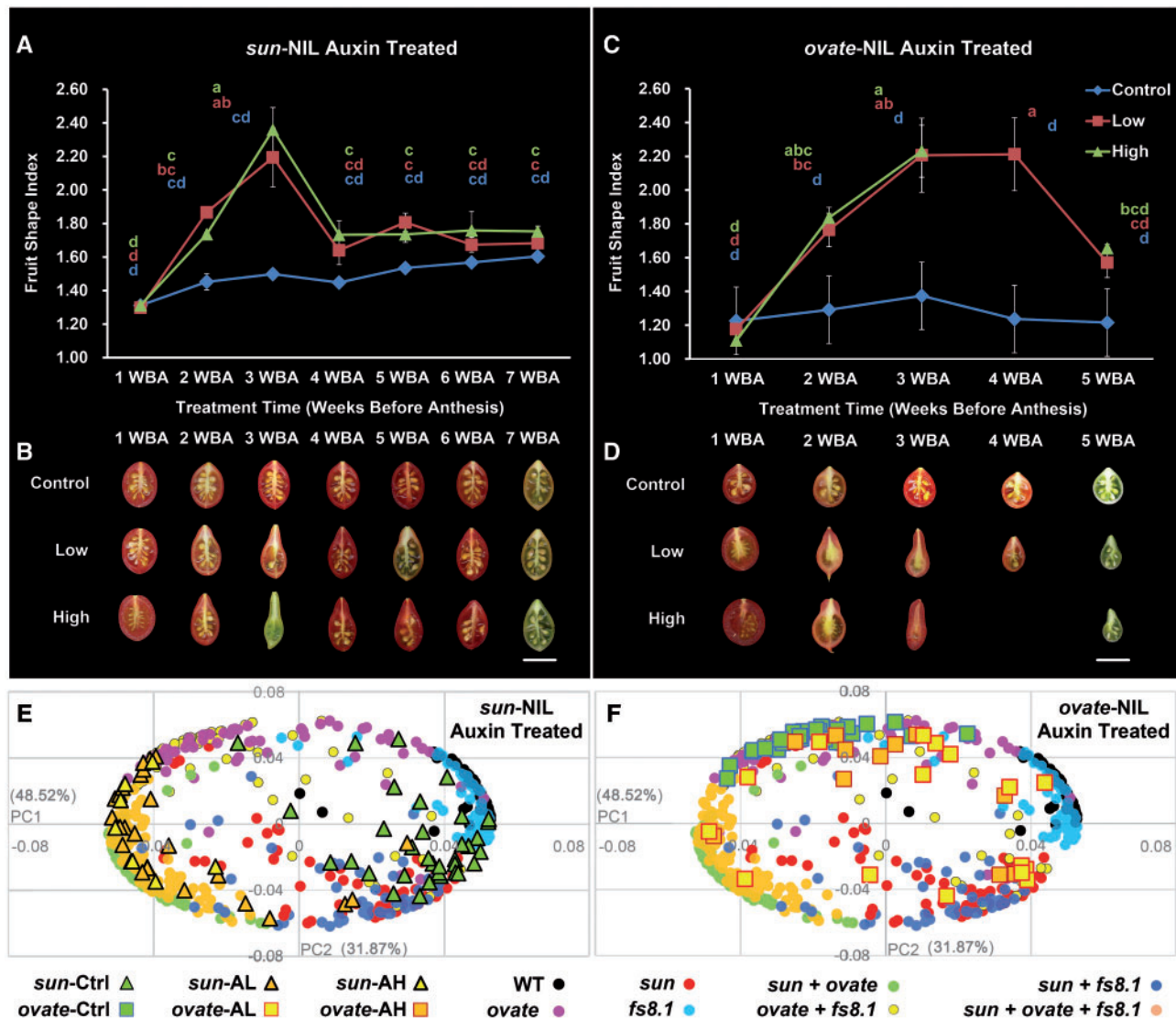


Fig. 3 Exogenous auxin elongated fruits of *sun* and *ovate* NILs in LA1589 background. (A, C) Fruit shape index changes after 2,4-D treatment in *sun* and *ovate* NILs. (B, D) Fruit shape changes after 2,4-D treatment in *sun* and *ovate* NILs. (E, F) PCA of fruit shape attributes in fruit shape NILs and 3 WBA auxin-treated *sun* and *ovate* NILs. Significant differences in (A) and (C) were evaluated using Tukey HSD tests at 0.05 level. Scale bars in (B) and (D) represented 1 cm. Ctrl, AL and AH in (E) and (F) represented control, low concentration of auxin and high concentration of auxin, respectively.

were clustered with those of *ovate*, *sun*, *sun+ovate* and *sun+ovate+fs8.1* NILs (Fig. 3F), implying a role of *sun*, *ovate* and auxin together in the regulation of fruit shape.

Exogenous auxin application changed the expression of *SUN* and *OVATE* in the inflorescence of WT NIL

We sought to test whether exogenous auxin application led to changes in the expression of the fruit shape genes. Using real-time PCR, expression of *SUN* was up-regulated by exogenous auxin application (>2-fold), whereas expression of *OVATE* was slightly up-regulated by the treatment (<2-fold) (Supplementary Fig. S3). The expression of four auxin response genes, namely *AUX19* (Solyc03g120380), *AUX17* (Solyc06g008590), *ARF5* (Solyc04g081235) and *ARF1* (Solyc01g103050), showed that the

first three genes were up-regulated, whereas the expression of the last gene was slightly down-regulated (Supplementary Fig. S3).

Expression analysis of tomato flower development in WT, *sun*, *ovate* and *fs8.1* NILs

sun, *ovate* and *fs8.1* affect ovary shape primarily by changing cell division patterns. To learn which genes accompany the changes in cell division, an RNA-seq analysis was performed with young flower buds at different developmental stages in WT, *sun*, *ovate* and *fs8.1* NILs. To obtain a general view of the transcriptome changes during flower development, a PCA was performed using the expression data from all the samples. In the dimensions defined by PC1 and PC2, which together explained more than 90% of the total variation, the samples were primarily clustered based on the developmental stage (Fig. 4A).

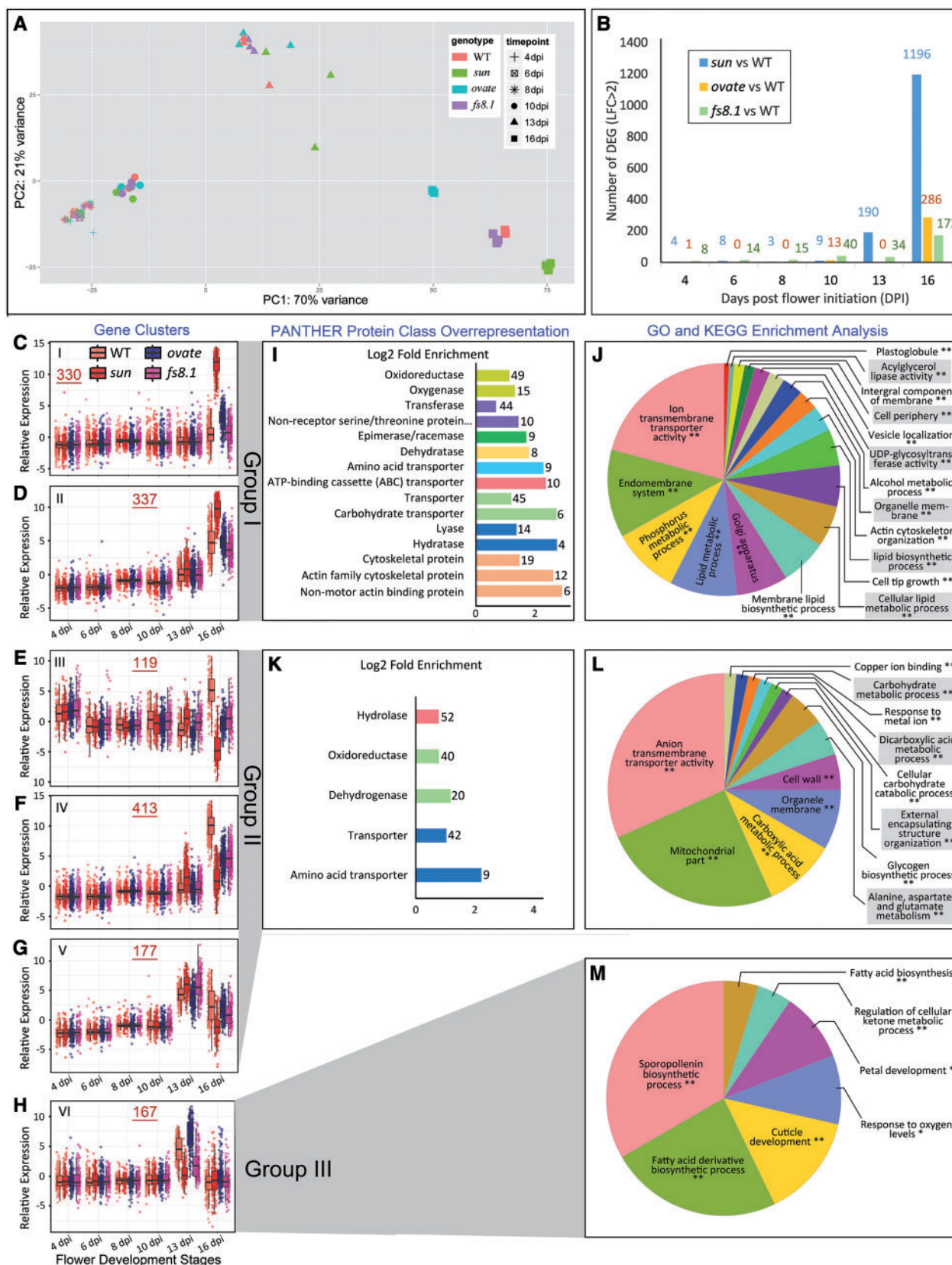


Fig. 4 Impact of *sun*, *ovate* and *fs8.1* on transcriptome of young flower buds at different developmental stages. (A) PCA plot of flower bud transcriptomes of WT, *sun*, *ovate* and *fs8.1* NILs. (B) Differentially expressed genes (DEGs) at different flower developmental stages in *sun*, *ovate* and *fs8.1* NILs. (C–H) Significantly differentially expressed genes affected by the interaction of genotype by developmental stages. (I, K) PANTHER protein class over-representation of genes in both class I and II. (J, L, M) GO and KEGG enrichment analyses of genes in class I, II and III. Number with underline in red color in (C–H) indicated the number of genes in each cluster.

Particularly at 4, 6, 8 and 10 DPI, samples for each stage were tightly clustered (Fig. 4A). In contrast, clusters of 13 and 16 DPI were not as tightly clustered and at 16 DPI, the samples from WT and *fs8.1* clustered together whereas the samples from *sun* and *ovate* clustered far apart from each other (Fig. 4A). The clustering at 16 DPI showed that expression profiles of the *ovate* and *sun* NILs were most distinct, whereas WT and *fs8.1* NIL were most similar to each other. For further insights into the effects of fruit elongation loci on flower bud transcriptomes, DEGs affected by the genotype were identified at each developmental stage (Fig. 4B). At the stages before 13 DPI, none of the fruit elongation loci showed a strong impact on gene expression (Fig. 4B). At 13 DPI, the expression of 190 genes was significantly changed by *sun*. At 16 DPI, the expression of many genes was significantly affected by all three loci (Fig. 4B). Venn diagram revealed that the highest number of common DEGs was found between *sun* and *ovate*, while, *ovate* and *fs8.1* shared the lowest number of common DEGs (Supplementary Fig. S4). DEGs affected by the genotype were enriched in many development-related GO, KEGG and PANTHER terms, and common cytoskeleton-related genes were enriched in *sun* and *ovate* (Supplementary Figs. S5, S6). It also appeared that the transcriptomes of flower buds were affected by both the genotype and the developmental stage. Thus, we sought to identify DEGs that were affected by the genotype \times developmental stage interaction using linear factorial modeling. The fuzzy C means clustering of the genotype \times developmental stage DEGs led to the identification of six tightly co-expressed clusters (Fig. 4C–H; Supplementary Table S1). Based on the effects of genotype, the six clusters were placed into three groups (Fig. 4C–H). Group I was comprised of cluster I and II, which represented genes that expressed at higher levels in *sun* NIL than in other NILs at 16 DPI (Fig. 4C, D). Group II was comprised of cluster III, IV and V, which represented genes that were up-regulated in WT compared to the other genotypes at 16 dpi (Fig. 4E–G). Group III was comprised of cluster VI, which represented genes that were up-regulated particularly in WT and *ovate* NILs at 13 DPI (Fig. 4H). The genes in each group were analyzed for the Gene Ontology enrichment analyses. Proteins encoded by the group I genes were classified into nine over-represented PANTHER protein classes (Fig. 4I). Group I genes were also found to be enriched in 18 GO and KEGG terms with the largest classes that were related to membrane-associated processes (Fig. 4J). In addition, proteins related to actin and cytoskeleton were enriched as well, which may be expected since SUN-like proteins are found to be associated with MT and MT-binding proteins (Bürstenbinder et al. 2013, Bürstenbinder et al. 2017). In group II, the deduced proteins were classified into three over-represented PANTHER classes and 13 GO and KEGG terms, some of which overlapped with those of the group I (Fig. 4I–L). Genes in group III showed enrichment in seven GO terms (Fig. 4M).

Fruit elongation loci affected the expression of auxin-related genes

We examined genes involved in auxin metabolism, homeostasis, polar transport and signal transduction to further explore the possible mechanistic link between auxin and fruit

elongation. From the RNA-seq data, 20 auxin-related genes were significantly differentially expressed either in a certain genotype at a certain developmental stage or by the genotype \times developmental stage interaction (Fig. 5A; Supplementary Fig. S7A–I). *sun* significantly affected the expression of 15 auxin-related genes, including *PIN5* (*Solyc01g068410*, encoding an auxin efflux transporter), *LAX3* (*Solyc11g013310*, encoding an auxin influx transporter), *ARF18* (*Solyc01g096070*, encoding an auxin response factor), two auxin-biosynthesis-related genes: *TAA1* (*Solyc05g031600*) and *YUCCA10* (*Solyc09g074430*), three *GH3s* (*Solyc02g092820*, *Solyc02g064830* and *Solyc07g053030*, encoding enzymes involving in auxin homeostasis) and five IAAAs (*Solyc09g090910*, *Solyc03g120380*, *Solyc06g084070*, *Solyc09g064530* and *Solyc03g121060*, encoding auxin signal repressors) at 16 DPI as well as *YUCCA6* (*Solyc08g068160*) and *ARF16B* (*Solyc10g086130*) at 13 and 16 DPI (Fig. 5A; Supplementary Fig. S7A–I). *ovate* significantly affected the expression of four auxin-related genes at 16 DPI, including *YUCCA6* (*Solyc08g068160*), *TAA1* (*Solyc05g031600*), *GH3-4* (*Solyc02g092820*) and *IAA2* (*Solyc06g084070*) (Fig. 5A; Supplementary Fig. S7A–C, G). *fs8.1* significantly changed the expression of eight auxin-related genes at 16 DPI, including *IAA29* (*Solyc08g021820*), *YUCCA11* (*Solyc09g074430*), *PIN5* (*Solyc01g068410*), *ARF16B* (*Solyc10g086130*) and four *GH3s* (*Solyc02g092820*, *Solyc02g064830*, *Solyc12g005310* and *Solyc01g068410*) (Fig. 5A; Supplementary Fig. S7B–D, G–I). As to the interaction of genotype \times developmental stage, it significantly affected the expression of seven genes, including two genes that belonged to group I (*GH3-6* and *ARF7*) and others that belonged to group II (*ARF17*, *IAA12*, *ARF16B*, *GH3-3* and *IAA14*) (Fig. 5A; Supplementary Fig. S7C, G–I). More integrally, compared with *ovate* and *fs8.1*, *sun* showed a stronger impact on differential gene expression of auxin-related genes, leading to their down-regulation compared to WT at later stages of floral development (Fig. 5B; Supplementary Fig. S7A–I).

Discussion

Fruit elongation by exogenous auxin application coincided with the earliest stages of gynoecium development

The gynoecium primordia arise approximately at 6 DPI, which is 14 d prior to flower opening (Xiao et al. 2009). Since the application of auxin started to influence fruit shape when applied 2 weeks before flower opening and with a stronger effect at 3 WBA, the hormone appeared to affect the shape well before the gynoecium primordia emergence (Figs. 1A, B, 3A–D). Consistent with that notion, the half-life of 2,4-D has been reported to be up to 20 d in nature and controlled environments (Voos and Groffman 1997, Chu 2001, Boivin et al. 2005), suggesting that one application can impact the entire developmental process of the gynoecium. In Arabidopsis, polar auxin transport as well as local auxin accumulation foci were observed between the carpel primordia initiation and carpel fusion (Larsson et al. 2014, Moubayidin and Østergaard 2014).

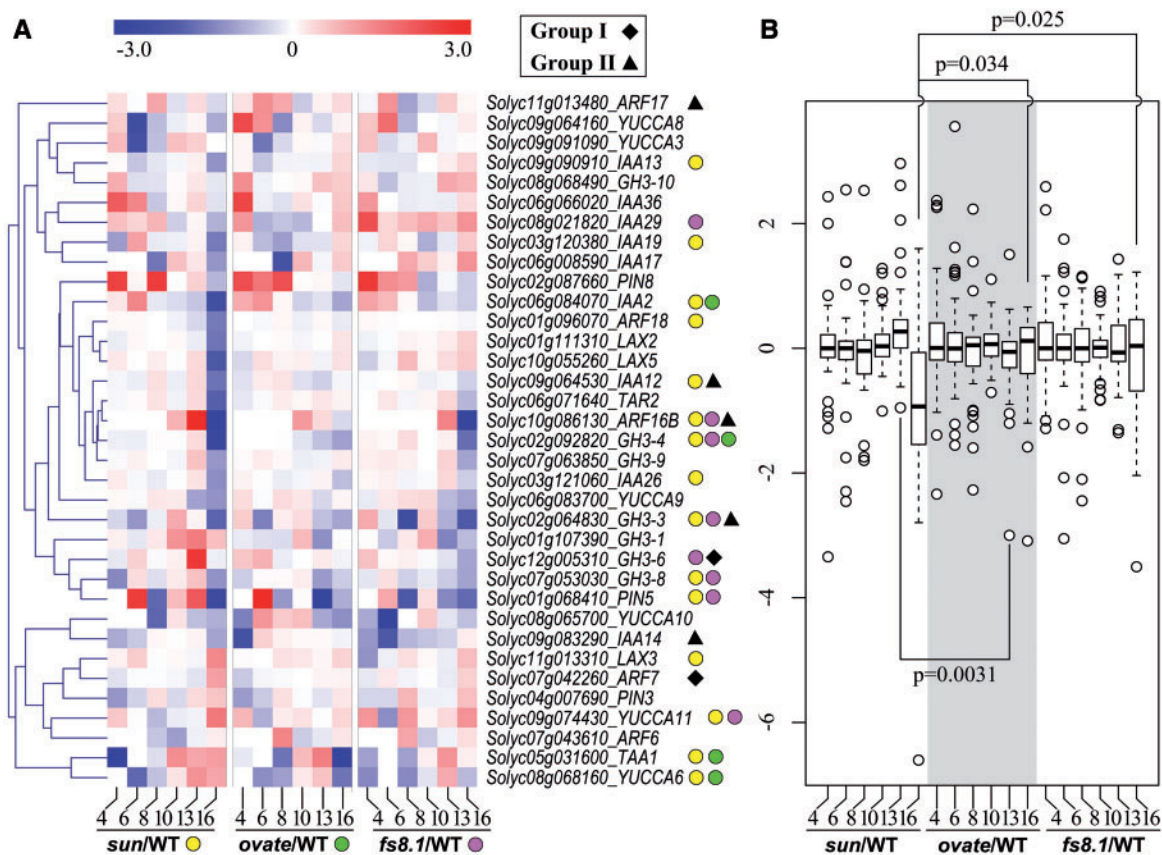


Fig. 5 Expression changes of auxin-related genes in flower buds of *sun*, *ovate* and *fs8.1* NILs at different development stages. (A) Expression changes of the expressed auxin-related genes in flower buds of *sun*, *ovate* and *fs8.1* NILs in comparison with the WT NIL at different development stages. Yellow, green and purple dots indicated significantly differentially expressed genes in *sun*, *ovate* and *fs8.1* NILs, respectively. Black diamonds and triangles indicated genes which were in group I and II in Fig. 4, respectively. (B) Boxplot of the expression changes of auxin-related genes in flower buds of *sun*, *ovate* and *fs8.1* NILs in comparison with the WT NIL at different development stages. Significant differences were evaluated using ANOVA pairwise comparisons.

Disturbances in auxin flow and accumulation led to abnormal gynoecia and siliques (Nemhauser et al. 2000, Sohlberg et al. 2006, Ståldal et al. 2008, Larsson et al. 2014, Moubayidin and Østergaard 2014), suggesting that this period is critical for the hormone to regulate the shape of gynoecium. Therefore, it is plausible that the tomato fruit elongation caused by exogenous auxin took place right before or during gynoecium primordia emergence.

Auxin, *sun* and *ovate* may share common genetic pathways in the regulation of tomato fruit shape

Plausible interactions between *SUN* and *OVATE* in the regulation of tomato fruit shape have been demonstrated in several prior studies (Wu et al. 2015, Lazzaro et al. 2018). Among those interactions, the most visible one is the elongated pear-shaped fruit. Interestingly, a pear shape is also the result of mutations in *OVATE* and *SIOFP20* (Wu et al. 2018) implying that this shape could be accomplished by different combination of genes. Genetic manipulation of *SUN* alone also lead to the pear-shaped fruit, as *SUN* overexpressing lines have shown (Supplementary Fig. S2B).

In this study, this particular shape was also produced by exogenous auxin application of WT inflorescences (Fig. 1B) and further enhanced in *sun* as well as in *ovate* NILs (Fig. 3B, D), suggesting a plausible link between auxin and *sun* and *ovate* in the regulation of tomato fruit shape. Based on visual and PCA evaluations, shapes of auxin-treated WT fruits were more similar to those of the *ovate* NIL than *sun* NIL (Fig. 1D), suggesting a tighter link between auxin and *ovate*. Further evidence supporting this notion came from the auxin-treated *sun* NILs which bore fruits that were similar in shape to *sun+ovate* NIL fruits from the PCA. Fruits of auxin-treated *ovate* NIL were even more pear-shaped (Fig. 3B, D–F) implying an enhancement of shape in *ovate* after auxin application. However, it should be noted that shapes of auxin-treated *sun* NIL fruits were also similar to those of *SUN* overexpressor lines (Fig. 3B; Supplementary Fig. S2B). The shape of auxin-treated *ovate* NIL fruits overlapped with those of *sun* NIL fruits in the PCA as well (Fig. 3F), suggesting the similar effect between auxin and *sun* in the regulation of tomato fruit. Therefore, it seemed that the morphological effect of exogenous auxin on tomato fruit shape was similar to those of *sun* and *ovate*,

indicating common genetic pathways may be employed by auxin, *sun* and *ovate* in the regulation of tomato fruit shape.

Possible mechanisms underlying the interactions among auxin, *sun* and *ovate* in the regulation of tomato fruit shape

Exogenous auxin application regulated the ovary shape by primarily changing directional cell number but also the cell size similar to *ovate* (Wu et al. 2018; **Table 2**), suggesting the elongation effect of this hormone may depend on changing the expression of *OVATE*. However, this hypothesis was not supported by *OVATE* expression analyses after auxin application (Supplementary Fig. S3). Since *OVATE* is a negative regulator of plant growth and overexpression of this gene leads to round fruit, slower plant growth and smaller compound-leaf size (Liu et al. 2002), the slight up-regulation of *OVATE* by exogenous auxin suggested that the elongation effect of this hormone on the tomato ovary and fruit shape may not be through the alteration of *OVATE* expression.

In another aspect, whether auxin was employed by *OVATE* to regulate ovary and fruit shape was still not clear. In a previous study, auxin level was not significantly changed in young flower buds in *ovate* NIL (Wu et al. 2015). On the other hand, *TAA1* and *YUCCA6* were down-regulated in developing flowers of the *ovate* NIL (**Fig. 5A**; Supplementary Fig. S7A, B), suggesting that the regulation of ovary and fruit shape by *OVATE* may not be through increasing the auxin level. Therefore, no direct link appears between auxin levels and expression of *OVATE* in the regulation of tomato fruit shape. Interestingly, a previous study has implied a link between auxin signaling and pear-shaped tomato fruits in miR160-knocked-down blocky-fruited M82 variety (Damodharan et al. 2016). miR160 fine-tunes auxin signaling by targeting three auxin response factors, *SIARF10* (Solyc11g069500 and Solyc06g075150), *SIARF16* (Solyc09g007810 and Solyc10g086130) and *SIARF17* (Solyc11g013470 and Solyc11g013480) (Damodharan et al. 2016). Unfortunately, none of the above genes were significantly differentially expressed in flower buds of *ovate* NIL (**Fig. 5A**), suggesting that the miR160-ARFs pathway did not use *OVATE* to regulate tomato fruit shape.

With regard to the interaction between auxin and *sun*, many studies suggested that this hormone may regulate tomato fruit shape mediated by *sun*. The phenotypes of vegetative and reproductive organs of *SUN* overexpressing lines are similar to those of the auxin mutants (Xiao et al. 2008, Wu et al. 2011, Hendelman et al. 2012, Damodharan et al. 2016). On the other hand, in this study, the pear-shaped seedless fruits of the auxin-treated *sun* and *ovate* NILs were similar to those of *SUN* overexpressors (**Fig. 3B, D**; Supplementary Fig. S2B). Moreover, among the three tomato fruit elongation loci, *sun* had the strongest impact on shifting the expression of the auxin-related genes, including those involved in auxin biosynthesis (*TAA*s and *YUCCA*s), homeostasis (*GH3*s), signal transduction (*IAA*s and *ARF*s) and polar transport (*PIN*s and *LAX*s) (**Fig. 5A, B**; Supplementary Fig. S7). Therefore, it seems that *sun* regulates fruit shape through affecting at least one or all of the processes controlled by auxin: metabolism, signal transduction and polar

transport. The cellular-based investigation implied that auxin regulated shape by increasing not only the cell number in the proximo-distal direction but also the cell size (**Table 2**; **Fig. 2**). However, cell size alteration was not observed in the *sun* NIL (**Table 2**). Also based on a previous study, the endogenous auxin level was not significantly changed in young inflorescences of *sun* NIL compared to WT (Wu et al. 2015). Consistent with that, although *sun* led to significantly increased expression of certain auxin biosynthesis genes, such as *TAA1*, *YUCCA6* and *YUCCA11* at 16 DPI, it also led to down-regulation of other members in the same family, such as *TAR2* and *YUCCA8* (**Fig. 5A**; Supplementary Fig. S7A, B). *sun* also led to an increase in the expression of *GH3-1*, a gene involved in auxin conjugation and homeostasis (Staswick et al. 2005, Domingo et al. 2009), at both 13 and 16 DPI (**Fig. 5A**; Supplementary Fig. S7C), which might together with the decrease in expression of *TAR2* and *YUCCA8* counteract the auxin level increase. Thus, we can assume that *SUN* may only employ the auxin signal transduction and/or polar transport processes, but not auxin level, to regulate tomato fruit shape.

As to the auxin polar transport and signaling, *sun* increased expression of *PIN8*, *LAX3* and *ARF7* at 16 DPI, but simultaneously down-regulated *PIN5*, *LAX2*, *LAX5*, *ARF16B*, *ARF18* as well as most of the *IAA*s (**Fig. 5A**; Supplementary Fig. S7D–I), suggesting a delicate fine-tuning of auxin transport and signaling at transcriptional level by *SUN*. Additionally, most of the *IAA*s were down-regulated at 16 DPI in *sun* NIL (**Fig. 5A**; Supplementary Fig. S7G). Since *IAA* genes encode repressors of auxin signaling and most of them are induced by auxin at the transcriptional level (Gray et al. 2001, Hagen and Guilfoyle 2002, Audran-Delalande et al. 2012), the down-regulation of *IAA*s could mean that the auxin level was not significantly increased. On the other hand, *sun* may regulate the shape via positively activating the auxin signaling pathway and the response genes through down-regulating the expression of *IAA* genes. *ARF16B* encodes one of the three *ARF*s targeted by miR160 (Damodharan et al. 2016). Contrary to *ovate*, *ARF16B* was significantly down-regulated at 16 DPI in *sun*; thus, it is possible that the miR160-*ARF* pathway may participate in the regulation of tomato fruit shape mediated by *sun* (**Fig. 5A**; Supplementary Fig. S7H, I).

The expression of *SUN* was clearly up-regulated by exogenous auxin treatment in the inflorescence of WT NIL (Supplementary Fig. S3), which was similar to certain *IQD* genes. In Arabidopsis, several *IQD* genes are potential targets of *ARF5* and the expression of *AtIQD15* increases after exogenous auxin application (Möller et al. 2017, Wendrich et al. 2018). Moreover, auxin treatment has also been shown to increase the cytosolic Ca^{2+} concentration, which may in turn regulate *IQD*'s function post-translationally by activation of Ca^{2+} /CaM signaling (Vanneste and Friml 2013), suggesting that auxin may regulate the ovary and fruit shape through direct interaction with *SUN* at transcriptional and/or post-transcriptional level. Additionally, certain *OFP*s interact with MT-associated proteins and may regulate MT structure and organization as well (Wu et al. 2018). A potential link between the *OFP*-TRM and *SUN*/*IQD* pathways has been discovered to associate with MT

assembling and rearrangement (Lazzaro et al. 2018). Therefore, it is possible that auxin may impact MT structure through the regulation of *SUN* at transcriptional and/or post-transcriptional level, which in turn changes cell division pattern resulting in the anisotropic growth of ovary, finally leading to a pear-shaped fruit which also involves *OFPs*.

It is also important to keep in mind that although exogenous auxin led to pear-shaped fruits in LA1589, changes of auxin level or signaling do not always lead to this particular shape. For example, overexpression of *SIARF2* (*Solyc03g118290*) in Micro-Tom (round fruit) resulted in obovoid (top heavy) fruits with elongated and restricted distal ends (De Jong et al. 2009); down-regulation of *SIARF7* (*Solyc07g042260*) in Moneymaker (flat fruit) and overexpression of a SI-miR160a-resistant version of *SIARF10* (*mSIARF10*, *Solyc11g069500*) in MP1 (round fruit) all led to parthenocarpic and heart-shaped fruits (Hendelman et al. 2012, Ren et al. 2017); in this study, applying 2,4-D to the WT NIL in Sun1642 background changed the fruits from round into rectangular shape (Supplementary Fig. S1B). Therefore, it is reasonable to assume that different factors in the auxin signal transduction pathway have distinct roles in remodeling organ shapes, and that responses to auxin may depend on the genetic background of plant materials.

Interrelationship of *sun*, *ovate* and *fs8.1* at the transcriptomic level during tomato floral development

In a previous study, significant additive effects were observed between *sun*, *ovate* and *fs8.1* in controlling the tomato fruit shape index (Wu et al. 2015). Further support of this notion comes from the histological analysis indicating that the three fruit elongation loci primarily affected cell number (Table 2). This implies that the additive effects in controlling the fruit shape index may be based on the cell number changes along the different development growth axis, which is controlled by the combination of two or all fruit elongation loci. In addition, *sun* impacts the morphology of most floral organs and leaves (Xiao et al. 2008, Wu et al. 2011, Wu et al. 2015). However, morphological changes have not been observed in the other floral organs in the *ovate* and *fs8.1* NILs (Sun et al. 2015, Wu et al. 2015). This suggests that *sun* has a broader role in organ shapes than *ovate* and *fs8.1*. Similarly, *sun* showed a stronger impact on the transcriptomes than *ovate* and *fs8.1*, since it showed the largest number of DEGs (Fig. 4B). Consistent with these findings are the genes that are significantly differentially expressed by the *sun* × development interaction (Fig. 4C–H). These genes were enriched in several important biological processes, such as lipid metabolism, ion transmembrane, actin cytoskeleton organization, carboxylic acid metabolic process, cell wall and UDP-glycosyltransferase (uridine 5'-diphospho-glucuronosyltransferase) (Fig. 4J–K), suggesting that *sun* had effects on many cellular processes. The analyses of transcriptomes and metabolites of young fruits also indicated that metabolites as well as genes related to TCA cycle, phytochromes and the cell wall were differentially accumulating (Clevenger et al. 2015). *OVATE* has been reported to

interact with certain members of TRM superfamily and is proposed to regulate cell division through interactions with MT, suggesting that the MT and its related factors may be common pathways shared by *SUN* and *OVATE* in the regulation of fruit shape (Van der Knaap et al. 2014, Wu et al. 2018). Interestingly, the potential link between *sun* and *ovate* was also reflected in the Venn diagram of DEGs and genotype, in which *ovate* shared much common DEGs with *sun* (52.7% of total DEGs of *ovate*) than with *fs8.1* (9.3% of total DEGs of *ovate*) (Supplementary Fig. S4). Meanwhile, as *fs8.1* shared more DEGs with *sun* (57.3% of total DEGs of *fs8.1*) than with *ovate* (12.3% of total DEGs of *fs8.1*) (Supplementary Fig. S4), it is reasonable to assume that *fs8.1* may share more common nodes or pathways with *sun* than with *ovate* in the regulation of tomato fruit shape at the molecular level.

Actin cytoskeleton organization genes may involve the *SUN*-mediated regulation of tomato fruit shape

Although lack of direct experimental evidence in tomato, based on the co-localization of IQDs in Arabidopsis, *SUN* is likely regulating cell division by the rearrangement of MT through recruiting CaMs to MT (Bürstenbinder et al. 2017). However, in this study, few MT-related genes were enriched or over-represented (Fig. 4I–M; Supplementary Figs. S5, S6). In contrast, several actin cytoskeleton organization genes were identified in both PANTHER protein class over-representation and GO and KEGG enrichment analyses (Fig. 4I–M; Supplementary Figs. S5, S6). As is well known, the cytoskeleton in plant cells comprises two major networks of protein polymers, actin microfilaments (AFs) and MTs, and many studies have pointed out that there is an interdependent crosstalk between AFs and MTs (Sampathkumar et al. 2011, Rosero et al. 2012, López et al. 2014, Schneider and Persson 2015, Tian et al. 2015). Thus, it is possible that actin cytoskeleton organization may be involved in the *SUN*-mediated regulation of tomato fruit shape. Consistence with this notion, several important AFs organization genes were up-regulated by *sun* at 16 DPI (Supplementary Table S1). Among those genes, *ACTINs* (*Solyc10g086460*, *Solyc04g011500* and *Solyc06g076090*), *ADFs* (*ACTIN DEPOLYMERIZING FACTORS*, *Solyc01g111380* and *Solyc09g072590*) and *RIC4* (*ROP-INTERACTIVE CRIB MOTIF-CONTAINING PROTEIN 4*, *Solyc11g008880*) lead to a dynamic equilibrium of actin polymerization and depolymerization events (Fu et al. 2005, Burgos-Rivera et al. 2008, Chang and Huang 2015, Chang et al. 2017, Zhu et al. 2017). Additionally, genes encoding homologs of Arabidopsis actin bundling and nucleation factors were also identified, including *AtVLN3* (*VILLIN 3*, *Solyc01g058210*), *AtWLIM1* (*Solyc11g044740*), *AtFH6* (*FORMIN HOMOLOG 6*, *Solyc02g092470*) and *AtFH5* (*Solyc07g06401*) (Supplementary Table S1). *AtFH5* is an actin nucleation factor that is associated with the cell plate in dividing cells and facilitating cytokinesis (Ingouff et al. 2005). *AtVLN3*, an actin-bundling protein, is essential for thick actin filament bundles and directional organ growth, and double mutant of *vln2 vln3* exhibit twisted leaves, stems, siliques and

roots which are similar to those of *SUN* overexpressors (Van der Honing et al. 2011, Bao et al. 2012). Moreover, certain AtVLNs are considered to have the Ca^{2+} /CaM-dependent actin bundling and severing activities (Zhang et al. 2011). Thus, an AFs regulatory network was constructed by those actin cytoskeleton organization genes, which regulated the AFs structure and dynamic equilibrium through Ca^{2+} /CaM-dependent and independent processes. This AFs regulatory network accompanied with MT-related processes may involve in the *SUN*-mediated regulation of tomato flower organ shape through controlling the cell division patterns.

Materials and Methods

Naming of the loci and alleles

The rules for the fruit shape loci and their mutant alleles are according to Wu et al. (2015): loci are italicized and in lowercase and the mutant alleles at the three fruit shape loci are named *sun*, *ovate* and *fs8.1*. Genes are referred to in capital letters and italicized whereas the proteins are referred to in capital letters.

Plant materials and growth conditions

NILs harboring all the combinations of *sun*, *ovate* and *fs8.1* alleles (WT, *sun*, *ovate*, *fs8.1*, *sun+ovate*, *sun+fs8.1*, *ovate+fs8.1*, *sun+ovate+fs8.1*) as homozygotes in *S. pimpinellifolium* LA1589 background were grown under standard greenhouse conditions at the Ohio Agricultural Research and Development Center (OARDC) in Wooster, OH, USA, in 2014 and 2015. Detailed information about the NILs was described previously (Wu et al. 2015).

Exogenous auxin treatments

Plants of WT, *sun* and *ovate* NILs were treated with 2,4-D (Sigma-Aldrich, USA, Cas#: 94–75-7), a synthetic auxin, when the first flower on the second inflorescence opened. Auxin application was performed using an auto-spray system with 2,4-D aqueous solutions (0 μM as control, 270 μM and 450 μM as treatments) at the speed of 94.64 l per 4,046.86 m^2/h (25 gallons per acre per hour). After treatment, plants were grown under standard greenhouse conditions and anthesis flowers were hand-pollinated every week and tagged. For each auxin concentration, at least 8 plants per genotype were used. In the WT NIL, the treatments were repeated twice.

Fruit shape measurement and principal component analysis

Fruits were collected at the mature green, orange or red stage, cut longitudinally, scanned at 300 dpi, and analyzed for fruit shape using Tomato Analyzer v3.0 according to the user manual (Rodríguez et al. 2010, http://vanderknaaplab.uga.edu/tomato_analyzer.html). Nine specific attributes were measured, including fruit shape index external I, fruit shape index external II, proximal fruit blockiness, distal fruit blockiness, fruit shape triangle, ellipsoid, circular, obovoid and width widest position. Definitions and measuring methods of the attributes were described in the user manual of Tomato Analyzer as well as our previous publications (Rodríguez et al. 2010, Wu et al. 2015). For each genotype or treatment, at least 20 fruits from more than 5 individual plants were evaluated. To compare the fruit shape among different NILs and auxin treatments, principal component analysis (PCA) was conducted using the `prcomp()` function in R with the 9 specific fruit shape attributes mentioned above. Before performing the PCA, data were mean centered and converted to their Z-score as described by Clevenger et al. (2015). Visualization of the PCA result was conducted using `ggplot()` in R.

Morphological and histological analyses of anthesis ovaries

Anthesis ovaries of WT, *sun* and *ovate* NILs were collected from the second, third and fourth inflorescences. Anthesis ovaries of the auxin-treated plants

were collected 3 weeks after treatment. Ultrathin resin-embedded sections of anthesis ovaries were performed in both proximal–distal and medio-lateral directions as described by Xiao et al. (2009) and Sun et al. (2015). Images were obtained using a Leica DM IRB microscope (Leica Microsystems, Germany) coupled to a CCD camera under a $\times 10$ objective lens. The entire ovary images were re-established with overlapping images using Photoshop CS5 (Adobe, USA) according to Sun et al. (2015). Ovary structure analysis, cell number and size measurements were conducted using ImageJ software (<http://rsbweb.nih.gov/ij/>) according to Sun et al. (2015). Fruit/ovary shape index is the ratio of fruit/ovary maximum length to the maximum width. Columella base and proximal end of ovary were indicated with purple and blue in Fig. 2A, respectively. For each genotype or treatment, at least five ovaries were sectioned, and for each ovary, three sections were analyzed.

Real-time PCR

Response of *SUN*, *OVATE*, *AUX19* (Solyc03g120380), *AUX17* (Solyc06g008590), *ARF1* (Solyc01g103050) and *ARF5* (Solyc04g081235) to 2,4-D was investigated in WT NIL using real-time PCR. Plants of WT NIL were grown in a greenhouse under standard condition at China Agricultural University, and the 2,4-D application was conducted when the first flower on the second inflorescence opened. RNA extraction, reverse transcription and real-time PCR were performed according to Sun et al. (2011). Primers were designed using Primer5 software and listed in Supplementary Table S2. *CAC*, *DNAJ* and *SAND* were selected as internal controls according to Expósito-Rodríguez et al. (2008). Relative expression values were calculated using $2^{-\Delta\Delta\text{CT}}$ method. For each gene, three technical repeats were performed, and the whole experiment was repeated twice. Boxplot of the expression data was conducted using `boxplot()` in R.

Sample collection, RNA library construction and sequencing

Transcriptome analysis of floral development was conducted in WT, *sun*, *ovate* and *fs8.1* NILs. The first inflorescences of each NIL were collected from approximately 150 3-week-old plants. In order to minimize the circadian effects on the transcriptome, inflorescences of all four NILs were collected at the same time each day within 2 h. The detached inflorescences were immediately immersed into 1 ml of ice-cooled RNAlater solution (Thermo Fisher Scientific, USA), and then vacuum infiltrated and stored at -20°C . Young flower buds at 4, 6, 8, 10, 13 and 16 days post-initiation of floral meristem (DPI) were separated and collected under a dissection microscope from the fixed inflorescences in the RNAlater solution. Developmental stage of young flower buds was determined by their positions on the inflorescence as described by Xiao et al. (2009). As flowering time and flower open time interval were not significantly affected by the three fruit elongation loci in this study (Supplementary Figs. S8, S9), flower buds collected from the same position of the inflorescence in different NILs could be considered at the same developmental stage. For stages 10, 13 and 16, at least 50 flower buds were collected for each replicate, and for other stages, the minimal collection number was 100. For each stage, a total of 2–4 replicates were collected. All the separated samples were stored in the RNAlater at -80°C before RNA extraction. Total RNA was extracted with Trizol (Invitrogen Inc., USA) as described by the manufacturer, and before the extraction, RNAlater was completely eliminated. RNA quantity and quality were assessed using an Agilent 2100 Bioanalyzer RNA 6000 Nano kit (Agilent, USA). Strand-specific RNA-seq libraries with insert size of approximately 250 bp were prepared according to Zhong et al. (2011) by starting with 2 μg total RNA. Libraries were barcoded, pooled and run on flowcells of the Illumina HiSeq2000 at the Genomics Resources Core Facility at Weill Cornell Medical College (New York, NY, USA). Single-end reads of 51 bp were generated.

RNA-seq data analysis

Gene expression value calculation and PCA. Illumina reads filtration, alignment and expression value calculation were carried out according to Huang et al. (2013) and Clevenger et al. (2015) by using Heinz1706 SL2.50 genome as reference. Gene expression value was represented as reads per kilobase of exon model per million mapped reads (RPKM). For clarifying the overall changes of the transcriptomes, PCA was conducted with expression profiles of

all the samples according to the method mentioned in the previous section. PCA result was plotted and edited using ggplot() in R and Photoshop CS5 (Adobe, USA), respectively.

Differential gene expression analysis. Differentially expressed genes (DEGs) caused by the genotype at each developmental stage were analyzed using the DESeq2 package as described by Anders et al. (2013) and Cleverger et al. (2015). *P*-values were adjusted using the Benjamini–Hochberg correction for multiple testing. For each genotype at a certain stage, biological replicates with correlation $\geq 99\%$ were used in the analysis and DEGs with an adjusted $P < 0.05$ were considered significant. A further filtration was performed to eliminate the low expressed genes. In this filtration, a gene with expression value larger than 2 RPKM in all two replicates, two out of three replicates or three out of four replicates was considered as an expressed gene.

In order to further clarify the effects of genotype and development on the gene expression patterns, differential expression analysis was also conducted using linear factorial modeling. Using DESeq2 and the function nbinomLRT(), null hypothesis whether each gene was affected by the interaction of genotype by developmental stage was tested.

Clustering of the DEGs during fruit development using fuzzy C means. The DEGs affected by the interaction of genotype by developmental stage were clustered using fuzzy C means by using the Mfuzz package (Futschik and Carlisle 2005) in R, with a C value of 100 to maximize dynamic differential clustering identification and core clustered at 0.70 membership probability. Gene clusters were visualized by plotting of the normalized expression profiles of each cluster using boxplot() in R.

Gene set enrichment analysis. Gene clusters generated from fuzzy C means were divided into groups based on the effect of genotype. Genes within each group were analyzed for enrichment using PANTHER Classification System (<http://pantherdb.org/>) and ClueGo App (Bindea et al. 2009) in Cytoscape v3.6.0 (<http://cytoscape.org/>). In PANTHER, genes' Solyc IDs were directly uploaded and statistical over-representation test was performed. Before being uploaded to ClueGo, tomato gene IDs were converted to Arabidopsis IDs using TAIR BLASTP (<https://www.arabidopsis.org/Blast/index.jsp>) according to Mu et al. (2017). Next, ClueGo analyses were run with the following settings: (i) GO Biological Process, GO Cellular Component, GO Molecular Function and KEGG were selected in Ontologies/Pathways option; (ii) Network Specificity was set as medium and their connectivity was based on a kappa score of 0.4; (iii) GO term fusion was set as true; (iv) Pathways with $P \leq 0.05$ were shown.

Expression analysis of auxin-related genes. Based on the BLAST results and gene's annotations, homologs of Arabidopsis auxin-related genes were identified from the tomato genome database, which includes genes involved in its metabolism, polar transport and signal transduction. Expression values of these auxin-related genes were extracted from the RNA-seq data. Pairwise comparisons of the expression values between the WT and mutant NILs at each developmental stage were conducted using Excel and the results were base-2 log transformed. Genes with expression value of less than 2 RPKM were filtered in all the tested samples. The final results were represented by a heatmap and a box-plot using MeV (mev.tm4.org) and boxplot() in R, respectively. ANOVA pairwise comparisons were accomplished using anova() in R.

Supplementary Data

Supplementary data are available at PCP online.

Funding

National Natural Science Foundation of China [31772319 to L.S.]; National Science Foundation [NSF IOS 0922661 to

E.v.d.K.]; 111 Project [B17043 to E.v.d.K.]; and Chinese Universities Scientific Fund [2018QC134 to L.S.].

Acknowledgments

We thank Jiheun Cho, Brenda Sanchez Montejo and Shin Reui Lee at OARDC, OSU, Wooster for taking care of the plants, Jason Van Houten for help with the analysis of the RNA-Seq data, Scott Wolfe and Dr. Roger Downer for help with the 2,4-D application; and Karolyne Kaszas at The Molecular and Cellular Imaging Center, OSU, Wooster for help with performing the resin section; and Jie Chen at China Agricultural University for help with conducting the Real-time PCR.

Disclosures

The authors have no conflicts of interest to declare.

References

- Anders, S., McCarthy, D., Chen, Y., Okoniewski, M., Smyth, G., Huber, W., et al. (2013) Count-based differential expression analysis of RNA sequencing data using R and Bioconductor. *Nat. Protoc.* 8: 1765–1786.
- Audran-Delalande, C., Bassa, C., Mila, I., Regad, F., Zouine, M. and Bouzayen, M. (2012) Genome-wide identification, functional analysis and expression profiling of the *AUX/IAA* gene family in tomato. *Plant Cell Physiol.* 53: 659–672.
- Bao, C., Wang, J., Zhang, R., Zhang, B., Zhang, H., Zhou, Y., et al. (2012) Arabidopsis *VILLIN2* and *VILLIN3* act redundantly in sclerenchyma development via bundling of actin filaments. *Plant J.* 71: 962–975.
- Bindea, G., Mlecnik, B., Hackl, H., Charoentong, P., Tosolini, M., Kirilovsky, A., et al. (2009) ClueGO: a cytoscape plug-in to decipher functionally grouped gene ontology and pathway annotation networks. *Bioinformatics* 25: 1091–1093.
- Biselli, C., Bagnaresi, P., Faccioli, P., Hu, X., Balcerzak, M., Mattered, M., et al. (2018) Comparative transcriptome profiles of near-isogenic hexaploid wheat lines differing for effective alleles at the 2DL FHB resistance QTL. *Front. Plant Sci.* 9: 37.
- Boivin, A., Amellal, S., Schiavon, M. and Van Genuchten, M.T. (2005) 2,4-Dichlorophenoxyacetic acid (2,4-D) sorption and degradation dynamics in three agricultural soils. *Environ. Pollut.* 138: 92–99.
- Burgos-Rivera, B., Ruzicka, D.R., Deal, R.B., McKinney, E.C., King-Reid, L. and Meagher, R.B. (2008) *ACTIN DEPOLYMERIZING FACTOR9* controls development and gene expression in *Arabidopsis*. *Plant Mol. Biol.* 68: 619–632.
- Bürstenbinder, K., Möller, B., Plötner, R., Stamm, G., Hause, G., Mitra, D., et al. (2017) The IQD family of calmodulin-binding proteins links calcium signaling to microtubules, membrane subdomains, and the nucleus. *Plant Physiol.* 173: 1692–1708.
- Bürstenbinder, K., Savchenko, T., Müller, J., Adamson, A.W., Stamm, G., Kwong, R., et al. (2013) *Arabidopsis* calmodulin-binding protein IQ67-domain 1 localizes to microtubules and interacts with kinesin light chain-related protein-1. *J. Biol. Chem.* 288: 1871–1882.
- Chakrabarti, M., Zhang, N.A., Sauvage, C., Muñoz, S., Blanca, J., Cañizares, J., et al. (2013) A cytochrome P450 regulates a domestication trait in cultivated tomato. *Proc. Natl. Acad. Sci. USA* 110: 17125–17130.
- Chang, M. and Huang, S. (2015) *Arabidopsis* ACT11 modifies actin turnover to promote pollen germination and maintain the normal rate of tube growth. *Plant J.* 83: 515–527.

- Chang, M., Li, Z. and Huang, S. (2017) Monomeric G-actin is uniformly distributed in pollen tubes and is rapidly redistributed via cytoplasmic streaming during pollen tube growth. *Plant J.* 92: 509–519.
- Chu, W. (2001) Modeling the quantum yields of herbicide 2,4-D decay in UV/H₂O₂ process. *Chemosphere* 44: 935–941.
- Clevenger, J., Van Houten, J., Blackwood, M., Gustavo, R.R., Jikumaru, Y., Kamiya, Y., et al. (2015) Network analyses reveal shifts in transcript profiles and metabolites that accompany the expression of *SUN* and an elongated tomato fruit. *Plant Physiol.* 168: 1164–1178.
- Damodharan, S., Zhao, D. and Arazi, T. (2016) A common miRNA160-based mechanism regulates ovary patterning, floral organ abscission and lamina outgrowth in tomato. *Plant J.* 86: 458–471.
- De Jong, M., Wolters-Arts, M., Feron, R., Mariani, C. and Vriezen, W.H. (2009) The *Solanum lycopersicum* auxin response factor 7 (*SIARF7*) regulates auxin signaling during tomato fruit set and development. *Plant J.* 57: 160–170.
- Domingo, C., Andrés, F., Tharreau, D., Iglesias, D.J. and Talón, M. (2009) Constitutive expression of *OsGH3.1* reduces auxin content and enhances defense response and resistance to a fungal pathogen in rice. *Mol. Plant-Microbe Interact.* 22: 201–210.
- Expósito-Rodríguez, M., Borges, A.A., Borges-Pérez, A. and Pérez, J.A. (2008) Selection of internal control genes for quantitative real-time RT-PCR studies during tomato development process. *BMC Plant Biol.* 8: 131.
- Eldridge, T., Langowski, Ł., Stacey, N., Jantzen, F., Moubayidin, L., Sicard, A., et al. (2016) Fruit shape diversity in the Brassicaceae is generated by varying patterns of anisotropy. *Development* 143: 3394–3406.
- Fu, Y., Gu, Y., Zheng, Z., Wasteneys, G. and Yang, Z. (2005) *Arabidopsis* interdigitating cell growth requires two antagonistic pathways with opposing action on cell morphogenesis. *Cell* 120: 687–700.
- Futschik, M.E. and Carlisle, B. (2005) Noise-robust soft clustering of gene expression time-course data. *J. Bioinform. Comput. Biol.* 3: 965–988.
- Goetz, M., Hooper, L.C., Johnson, S.D., Rodrigues, J.C.M., Vivian-Smith, A. and Koltunow, A.M. (2007) Expression of aberrant forms of *AUXIN RESPONSE FACTOR8* stimulates parthenocarpy in *Arabidopsis* and tomato. *Plant Physiol.* 145: 351–366.
- Gray, W.M., Kepinski, S., Rouse, D., Leyser, O. and Estelle, M. (2001) Auxin regulates SCF^{TRT1}-dependent degradation of AUX/IAA proteins. *Nature* 414: 271.
- Hagen, G. and Guilfoyle, T. (2002) Auxin-responsive gene expression: genes, promoters and regulatory factors. *Plant Mol. Biol.* 49: 373–385.
- Hendelman, A., Buxdorf, K., Stav, R., Kravchik, M. and Arazi, T. (2012) Inhibition of lamina outgrowth following *Solanum lycopersicum* *AUXIN RESPONSE FACTOR 10* (*SIARF10*) derepression. *Plant Mol. Biol.* 78: 561–576.
- Huang, Z., Van Houten, J., Gonzalez, G., Xiao, H. and van der Knaap, E. (2013) Genome-wide identification, phylogeny, and expression analysis of *SUN*, *OPF* and *YABBY* gene family in tomato. *Mol. Genet. Genomics* 288: 111–129.
- Ingouff, M., Gerald, J.N.F., Guérin, C., Robert, H., Sørensen, M.B., Van Damme, D., et al. (2005) Plant formin AtFH5 is an evolutionarily conserved actin nucleator involved in cytokinesis. *Nat. Cell Biol.* 7: 374.
- Larsson, E., Roberts, C., Claes, A., Franks, R.G. and Sundberg, E. (2014) Polar auxin transport is essential for medial versus lateral tissue specification and vascular-mediated valve outgrowth in *Arabidopsis* gynoecia. *Plant Physiol.* 166: 1998–2012.
- Lazzaro, M.D., Wu, S., Snouffer, A., Wang, Y. and Van Der Knaap, E. (2018) Plant organ shapes are regulated by protein interactions and associations with microtubules. *Front. Plant Sci.* 9: 1766.
- Liu, J., Van Eck, J., Cong, B. and Tanksley, S.D. (2002) A new class of regulatory genes underlying the cause of pear-shaped tomato fruit. *Proc. Natl. Acad. Sci. USA* 99: 13302–13306.
- López, M.P., Huber, F., Grigoriev, I., Steinmetz, M.O., Akhmanova, A., Koenderink, G.H., et al. (2014) Actin-microtubule coordination at growing microtubule ends. *Nat. Commun.* 5: 4778.
- Möller, B.K., Colette, A., Xiang, D., Williams, N., López, L.G., Yoshida, S., et al. (2017) Auxin response cell-autonomously controls ground tissue initiation in the early *Arabidopsis* embryo. *Proc. Natl. Acad. Sci. USA* 114: E2533–E2539.
- Moubayidin, L. and Østergaard, L. (2014) Dynamic control of auxin distribution imposes a bilateral-to-radial symmetry switch during gynoecium development. *Curr. Biol.* 24: 2743–2748.
- Mu, Q., Huang, Z., Chakrabarti, M., Illa-Berenguer, E., Liu, X., Wang, Y., et al. (2017) Fruit weight is controlled by cell size regulator encoding a novel protein that is expressed in maturing tomato fruits. *PLoS Genet.* 13: e1006930.
- Muños, S., Ranc, N., Botton, E., Bérard, A., Rolland, S., Duffé, P., et al. (2011) Increase in tomato locule number is controlled by two SNPs located near *WUSCHEL*. *Plant Physiol.* 156: 2244–2254.
- Nemhauser, J.L., Feldman, L.J. and Zambryski, P.C. (2000) Auxin and ETTIN in *Arabidopsis* gynoecium morphogenesis. *Development* 127: 3877–3888.
- Ren, Z., Liu, R., Gu, W. and Dong, X. (2017) The *Solanum lycopersicum* auxin response factor *SIARF2* participates in regulating lateral root formation and flower organ senescence. *Plant Sci.* 256: 103–111.
- Rodríguez, G.R., Kim, H.J. and Van der Knaap, E. (2013) Mapping of two suppressors of *OVATE* (*sov*) loci in tomato. *Heredity (Edinb)* 111: 256.
- Rodríguez, G.R., Moysenko, J.B., Robbins, M.D., Morejón, N.H., Francis, D.M. and Van der Knaap, E. (2010) Tomato Analyzer: a useful software application to collect accurate and detailed morphological and colorimetric data from two-dimensional objects. *J. Vis. Exp.* 37: 1856.
- Rosero, A., Žárský, V. and Cvrčková, F. (2012) AtFH1 formin mutation affects actin filament and microtubule dynamics in *Arabidopsis thaliana*. *J. Exp. Bot.* 64: 585–597.
- Sampathkumar, A., Lindeboom, J.J., Debolt, S., Gutierrez, R., Ehrhardt, D.W., Ketelaar, T., et al. (2011) Live cell imaging reveals structural associations between the actin and microtubule cytoskeleton in *Arabidopsis*. *Plant Cell* 23: 2302–2313.
- Schneider, R. and Persson, S. (2015) Connecting two arrays: the emerging role of actin-microtubule cross-linking motor proteins. *Front. Plant Sci.* 6: 415.
- Sohlberg, J.J., Myrenäs, M., Kuusk, S., Lagercrantz, U., Kowalczyk, M., Sandberg, G., et al. (2006) *STY1* regulates auxin homeostasis and affects apical-basal patterning of the *Arabidopsis* gynoecium. *Plant J.* 47: 112–123.
- Ståldal, V., Sohlberg, J.J., Eklund, D.M., Ljung, K. and Sundberg, E. (2008) Auxin can act independently of *CRC*, *LUG*, *SEU*, *SPT* and *STY1* in style development but not apical-basal patterning of the *Arabidopsis* gynoecium. *New Phytol.* 180: 798–808.
- Staswick, P.E., Serban, B., Rowe, M., Tiryaki, I., Maldonado, M.T., Maldonado, M.C., et al. (2005) Characterization of an *Arabidopsis* enzyme family that conjugates amino acids to indole-3-acetic acid. *Plant Cell* 17: 616–627.
- Sun, L., Chen, J., Xiao, K. and Yang, W. (2017) Origin of the domesticated horticultural species and molecular bases of fruit shape and size changes during the domestication, taking tomato as an example. *Hortic. Plant J.* 3: 125–132.
- Sun, L., Rodríguez, G.R., Clevenger, J.P., Illa-Berenguer, E., Lin, J., Blakeslee, J.J., et al. (2015) Candidate gene selection and detailed morphological evaluations of *fs8.1*, a quantitative trait locus controlling tomato fruit shape. *J. Exp. Bot.* 66: 6471–6482.
- Sun, L., Wang, Y.P., Chen, P., Ren, J., Ji, K., Li, Q., et al. (2011) Transcriptional regulation of *SIPYL*, *SIPP2C*, and *SISnRK2* gene families encoding ABA signal core components during tomato fruit development and drought stress. *J. Exp. Bot.* 62: 5659–5669.
- Tian, J., Han, L., Feng, Z., Wang, G., Liu, W., Ma, Y., et al. (2015) Orchestration of microtubules and the actin cytoskeleton in trichome cell shape determination by a plant-unique kinesin. *Elife* 4: e09351.
- Van der Honing, H., Kieft, H., Emons, A.M. and Ketelaar, T. (2011) *Arabidopsis* *VILLIN2* and *VILLIN3* are required for the generation of thick actin filament bundles and for directional organ growth. *Plant Physiol.* 158: 1426–1438.

- Van der Knaap, E., Chakrabarti, M., Chu, Y.H., Clevenger, J.P., Illa-Berenguer, E., Huang, Z., et al. (2014) What lies beyond the eye: the molecular mechanisms regulating tomato fruit weight and shape. *Front. Plant Sci.* 5: 227.
- Van der Knaap, E. and Østergaard, L. (2017) Shaping a fruit: developmental pathways that impact growth patterns. *Semin. Cell Dev. Biol.* 79: 27–36.
- Vanneste, S. and Friml, J. (2013) Calcium: the missing link in auxin action. *Plants (Basel)* 2: 650–675.
- Voos, G. and Groffman, P.M. (1997) Dissipation of 2,4-D and dicamba in a heterogeneous landscape. *Appl. Soil. Ecol.* 5: 181–187.
- Wang, H., Jones, B., Li, Z., Frasse, P., Delalande, C., Regad, F., et al. (2005) The tomato *Aux/IAA* transcription factor *IAA9* is involved in fruit development and leaf morphogenesis. *Plant Cell* 17: 2676–2692.
- Wendrich, J., Yang, B.J., Mijnhout, P., Xue, H.W., De Rybel, B. and Weijers, D. (2018) IQD proteins integrate auxin and calcium signaling to regulate microtubule dynamics during *Arabidopsis* development. <https://doi.org/10.1101/275560>.
- Wu, S., Clevenger, J.P., Sun, L., Visa, S., Kamiya, Y., Jikumaru, Y., et al. (2015) The control of tomato fruit elongation orchestrated by *sun*, *ovate* and *fs8.1* in a wild relative of tomato. *Plant Sci.* 238: 95–104.
- Wu, S., Xiao, H., Cabrera, A., Meulia, T. and Van der Knaap, E. (2011) *SUN* regulates vegetative and reproductive organ shape by changing cell division patterns. *Plant Physiol.* 157: 1175–1186.
- Wu, S., Zhang, B., Keyhaninejad, N., Rodríguez, G.R., Kim, H.J., Chakrabarti, M., et al. (2018) A common genetic mechanism underlies morphological diversity in fruits and other plant organs. *Nat. Commun.* 9: 4734.
- Xiao, H., Jiang, N., Schaffner, E., Stockinger, E.J. and Van Der Knaap, E. (2008) A retrotransposon-mediated gene duplication underlies morphological variation of tomato fruit. *Science* 319: 1527–1530.
- Xiao, H., Radovich, C., Welty, N., Hsu, J., Li, D., Meulia, T., et al. (2009) Integration of tomato reproductive developmental landmarks and expression profiles, and the effect of *SUN* on fruit shape. *BMC Plant Biol.* 9: 49.
- Zhang, Y., Xiao, Y., Du, F., Cao, L., Dong, H. and Ren, H. (2011) *Arabidopsis* VILLIN4 is involved in root hair growth through regulating actin organization in a Ca^{2+} -dependent manner. *New Phytol.* 190: 667–682.
- Zhong, S., Joung, J.G., Zheng, Y., Chen, Y.R., Liu, B., Shao, Y., et al. (2011) High-throughput illumina strand-specific RNA sequencing library preparation. *Cold Spring Harb. Protoc.* 2011: 5652.
- Zhu, J., Nan, Q., Qin, T., Qian, D., Mao, T., Yuan, S., et al. (2017) Higher-ordered actin structures remodeled by *Arabidopsis* ACTIN-DEPOLYMERIZING FACTOR5 are important for pollen germination and pollen tube growth. *Mol. Plant* 10: 1065–1081.